J|A|C|S
ARTICLES
Published on Web 12/27/2001

Magnetic Field-Controlled Microfluidic Transport

Kyle M. Grant, Jared W. Hemmert, and Henry S. White*

Contribution from the Department of Chemistry, University of Utah, Salt Lake City, Utah 84112

Received July 4, 2001

Abstract: Several new forms of magnetohydrodynamic (MHD) flow occurring in the solution gap between two 250-μm-diameter Pt microdisk electrodes, oriented in a face-to-face geometry and immersed in a uniform magnetic field (1 T), are described. The MHD flow results from the Lorentz force generated by diffusion of electrochemically generated molecular ions through the magnetic field. Individual microscopic flow tubes ($\sim$50-μm radius) spanning the gap between the face-to-face electrodes are observed during the 1-e$^-$ reduction of nitrobenzene in acetonitrile solutions. The flow tubes extend up to $\sim$2 cm in length and are stable for indefinite periods. Directional transport of the electrogenerated nitrobenzene radical anion over macroscopic distances within the flow tubes, with minimal diffusional broadening, is demonstrated using an ultramicroelectrode probe to map the convective flux of redox species. Pulsed MHD transport of small packets of molecules and the formation of large area ($\sim$3 cm^2), microscopically thin (25 μm) rotating sheets of solution are also demonstrated. The results suggest that electrochemical methods, in combination with magnetohydrodynamic principles, may be useful for external field-controlled microfluidic systems.

Introduction

We wish to report the use of magnetic fields for confinement and directional transport of molecules in a condensed fluid phase. Confinement and acceleration of ions using magnetic and/or electric fields has a long history of application in physics and chemistry and forms the basis for several methods of gas-phase chemical analysis (e.g., ion cyclotron resonance mass spectrometry[1]). In liquids, short-range interactions between neighboring molecules prohibit the acceleration of individual molecules over significant distances before collisions randomize the direction of motion.[2] Directional transport of molecular species in liquids is thus accomplished by the use of rigid confining surfaces, such as microfluidic channels that are under current study in chemical synthesis[3,4] and microanalysis.[5−7] Our objective here is to illustrate a new fundamental approach for transport of molecules over macroscopic length scales in viscous liquids, using an external magnetic field to prevent diffusional broadening.

The strategy reported herein involves magnetohydrodynamic (MHD) solution flow engendered by the diffusion of electrochemically generated molecules through an externally applied and uniform magnetic field. Earlier reports from this laboratory have demonstrated the ability to establish well-defined MHD flows within nanoliter volumes of solution adjacent to electrodes of micrometer and submicrometer diameters.[8−15] Significant enhancement in the transport-controlled electrochemical currents (up to 400% increase[11]) can be induced by local MHD flow, a result of rapid convective transport of the redox reactant to the microelectrode surface.

MHD flow in solution results from the Lorentz force acting on ions as they move through the magnetic field, similar to the force experienced by an electron or ion moving through a magnetic field in a vacuum.[16,17] In the absence of electrical fields, the Lorentz force is given by $\mathbf{F} = q(\boldsymbol{v} \times \mathbf{B})$, where q is the charge on the ion, $\boldsymbol{v}$ is the velocity, and $\mathbf{B}$ is the externally applied magnetic field. Numerous examples of MHD flow driven by electrochemical currents at *macroscopic* electrodes have been reported in the literature.[18−41] Since a large ensemble

* To whom correspondence should be addressed. E-mail: white@chemistry.utah.edu.

(1) Marshall, A. G.; Hendrickson, C. L.; Jackson, G. S. *Mass Spectrom. Rev.* **1998**, 17, 1−35.
(2) Berg, H. C. *Random Walks in Biology*; Princeton University Press: Princeton, NJ, 1983.
(3) Kenis, P. J. A.; Ismagilov, R. F.; Takayama, S.; Whitesides, G. M.; Li, S.; White, H. S. *Acc. Chem. Res.* **2000**, *33*, 841−847.
(4) Kenis, P. J. A.; Ismailov, R. F.; Whitesides, G. M. *Science* **1999**, *285*, 83−85.
(5) Harrison, J. D. *Science* **1993**, *261*, 895.
(6) Strolmberg, A.; Karlsson, A.; Ryttse'n, F.; Davidson, M.; Chiu, D. T.; Orwar, O. *Anal. Chem.* **2001**, *73*, 126−130.
(7) Barker, S. L. R.; Ross, D.; Tarlov, M. J.; Gaitan, M.; Locascio, L. E. *Anal. Chem.* **2000**, *72*, 5925−5929.
(8) Grant, K. M.; Hemmert, J. W.; White, H. S. *J. Electroanal. Chem.* **2001**, *500*, 95−99.
(9) Grant, K. M.; Hemmert, J. W.; White, H. S. *Electrochem. Com.* **1999**, *1*, 319−323.
(10) Ragsdale, S. R.; White, H. S. *Anal. Chem.* **1999**, *71*, 1923−1927.
(11) Ragsdale, S. R.; Grant, K. M.; White, H. S. *J. Am. Chem. Soc.* **1998**, *120*, 13461−13468.
(12) Ragsdale, S. R.; Lee, J.; White, H. S. *Anal. Chem.* **1997**, *69*, 2070−2076.
(13) Ragsdale, S. R.; Lee, J.; Gao, X.; White, H. S. *J. Phys. Chem.* **1996**, *100*, 5913−5922.
(14) Lee, J.; Ragsdale, S.; Gao, X.; White, H. S. *J. Electroanal. Chem.* **1997**, *442*, 169−177.
(15) Lee, J.; Gao, X.; Hardy, L. D. A.; White, H. S. *J. Electrochem. Soc.* **1995**, *142*, L90−L92.
(16) Feynman, R. P.; Leighton, R. B.; Sands, M. L. *The Feynman Lectures on Physics*; Addison-Wesley: Reading, MA, 1964; Vol. 2.
(17) Griffiths, D. J. *Introduction to Electrodynamics*, 3rd ed.; Prentice Hall: Upper Saddle River, NJ, 1999.
(18) Fahidy, T. J. *Chem. Eng. J.* **1974**, *7*, 21−27.
(19) Fahidy, T. Z. *J. Appl. Electrochem.* **1983**, *13*, 553−563.
(20) Leventis, N.; Chen, M.; Gao, X.; Canalas, M.; Zhang, P. *J. Phys. Chem.* **1998**, *102*, 3512−3522.
(21) Fahidy, T. Z. *Modern Aspects of Electrochemistry: The Effect of Magnetic Fields on Electrochemical Processes*; Kluwer Academic: New York, 1999; Vol. 32.

10.1021/ja016544y CCC: $22.00

of ions is in motion in electrochemical systems, including both the redox-active molecules and inert electrolyte ions, the driving force for MHD flow may be more conveniently expressed as a force density,[17] $\mathbf{F}_{MHD}$ (N/m^3), acting on an infinitesimal volume of the solution. In eq 1, $\mathbf{J}$ (C/m^2s) is the local net flux of current-carrying species. Transfer of momentum from the field-accelerated ions to the solution by viscous interactions gives rise to MHD flow, as described by the Navier−Stokes equation (vide infra).[20,42]

$$\mathbf{F}_{MHD} = \mathbf{J} \times \mathbf{B} \quad (1)$$

In a uniform field (i.e., $\mathbf{B}$ constant), eq 1 indicates that the direction of the magnetic force, $\mathbf{F}_{MHD}$, and, thus, the resulting MHD flow are determined solely by the magnitude and direction of the net flux of current-carrying species. This relationship is key to our strategy for creating novel MHD flow patterns, since the current density distribution at microelectrodes can be varied in a nearly arbitrary fashion by varying the shape and size of the electrode.[43,44] In addition, and most importantly, two or more microelectrodes can be placed close to one another using micropositioning techniques, creating novel MHD flows that are not obtainable with an individual electrode.

Herein, we demonstrate that microscopic MHD flow tubes, generated in a dual-electrode configuration, can be used to transport molecules over macroscopic distances in a condensed phase without significant loss due to diffusional broadening or convective mixing. Analogous "liquid beams" prepared by continuous pressure-driven flow of liquid through a small nozzle into a vacuum have been recently reported by Kohno and co-workers.[45,46] In addition to the MHD flow tubes, we also described pulsed MHD transport, in which a small number of molecules are generated and transported as a packet across the solution, and an example of free-standing MHD sheet flow. Our results illustrate the variety of novel MHD flows that can be engineered using microelectrode techniques.

Experimental Section

Chemicals. Tetra-*n*-butylammonium hexafluorophosphate, [*n*-Bu_4N]-PF_6 (Sigma), was recrystallized three times from ethylacetate/ethanol and dried under a vacuum. Nitrobenzene (NB, Aldrich, 99%) and acetonitrile (CH_3CN, Fisher Scientific, HPLC grade) were stored over 4-Å molecular sieves. 2-Allylphenol (Aldrich), 2-butoxyethanol (Aldrich), and ammonium hydroxide (Mallinckrodt AR) were used as received.

Electrochemical Measurements. Inlaid-disk Pt microelectrodes were prepared by sealing one end of a 250-μm-radius Pt wire (Alfa AESAR, 99.998%) in a 5-mm-o.d. glass tube using a H_2/O_2 torch. The sealed end was sanded flat to expose a disk-shaped Pt surface shrouded in glass. Electrodes were polished with 1.5, 0.3, and 0.01 μm alumina, rinsed with water, and briefly sonicated in methanol to remove polishing debris.

MHD flow in the gap between two 250-μm-radius microdisk electrodes was characterized using a 25-μm-radius Pt microprobe electrode to measure the spatial distributions of the electrochemical reactant and product. The microprobe electrode was constructed using a polymer coating procedure developed by Potje-Kamloth et al.[47] An 8-mm length of a 25-μm-radius Pt wire (Alfa Aesar 99.9995%) was connected to a Cu wire and sealed in 2.0-mm-o.d. glass tubing, leaving 3−4 mm of the wire exposed. An insulating film of polyphenylene oxide was electrodeposited onto the exposed metal surface by biasing the electrode for 30 min at a potential of 4.0 V vs Ag/AgCl in a methanol/water (50:50) solution of 0.4 M 2-allylphenol, 0.4 M 2-butoxyethanol, and 0.4 M ammonium hydroxide. The polymer film was initially cured at 110 °C for 75 min and then at 170 °C for 5 h. The insulating properties of the polymer coating were tested by recording the voltammetric response of the coated wire in an CH_3CN solution containing 2.0 mM ferrocene. No measurable currents were observed, indicating that the thin polymer film effectively insulates the Pt surface. The end of the wire was then cut to expose a quasi-disk-shaped Pt surface. A sigmoid-shaped voltammogram was observed in the CH_3CN/ferrocene solution after the wire was cut, consistent with the expected microdisk geometry.

Voltammetric measurements were performed using a three-neck glass cell (open to air). Potentials of the 250-μm-radius Pt electrodes were controlled using a Pine Instrument Co. RDE4 bipotentiostat. Voltammetric data at the smaller microprobe Pt electrode were obtained using a Bioanalytical Systems CV-27 potentiostat. The Ag/Ag_xO quasi-reference electrode used in this study was prepared before each experiment by dipping a clean Ag wire in concentrated nitric acid for ~5 s, rinsing with H_2O, and drying at 110 °C. All electrode potentials are reported versus the Ag/Ag_xO electrode, which was measured to be ~ −0.13 V vs a saturated calomel reference electrode. The auxiliary electrode was a Pt wire. Voltammetric data were recorded by use of virtual instrumentation software written with National Instruments LabVIEW.

Magnetohydrodynamic Flow Experiments. A benchtop electromagnet with 7.6-cm diameter poles separated by ~2 cm (GMW Associates model 5403) was employed to generate a uniform 1.0-T magnetic field across the electrochemical cell. The electromagnet, field uniformity, and applications in electrochemical investigations have been described elsewhere in detail.[13,14] The magnetic field strength was varied between 0 and 1 T by adjusting the current to the electromagnet. Field strengths were measured using a gauss meter (F. W. Bell, model 4048).

Positioning of the two 250-μm-radius microdisk electrodes and the 25-μm-radius microprobe electrode with ~1-μm precision was performed by use of one-dimensional axis modular translation stages and

(22) Leventis, N.; Gao, X. *J. Phys. Chem. B* **1999**, *103*, 5832−5840.
(23) Aogaki, R.; Fueki, K.; Mukaibo, T. *Denki Kagaku* **1975**, *43*, 509−514.
(24) Aogaki, R.; Negishi, T.; Yamato, M.; Ito, E.; Mogi, I. *Phyisca B* **1994**, *210*, 611−615.
(25) Devos, O.; Aogaki, R. *Anal. Chem.* **2000**, *72*, 2835−2840.
(26) Aaboudi, O.; Chopart, J. P.; Douglade, J.; Olivier, A.; Gabrielli, C.; Tribollet, B. *J. Electrochem. Soc.* **1990**, *137*, 1796−1804.
(27) Wakaas, M.; Kharkats, Y. I. *J. Phys. Chem.* **1999**, *103*, 4876−4883.
(28) Bobreshova, O. V.; Golitsyn, V. Y.; Timashev, S. F. *Soviet Electrochem.* **1990**, *26*, 50−54.
(29) Leilmezs, J.; Musbally, G. M. *Electrochemica Acta* **1972**, *17*, 1609−1613.
(30) Kelly, E. *J. Electrochem. Soc.* **1977**, *124*, 987−994.
(31) Wakasa, M.; Sakaguchi, Y.; Hayashi, H. *Chem. Lett.* **1994**, 49−50.
(32) Tacken, R. A.; Janssen, L. J. J. *J. Appl. Electrochem.* **1995**, *25*, 1−5.
(33) Oliver, A.; Chopart, J. P.; Douglade, J. *J. Electroanal. Chem.* **1987**, *217*, 443.
(34) Katsuki, A.; Wantanabe, R.; Tokunaga, R.; Tanimoto, Y. *Chem. Lett.* **1996**, *24*, 219−220.
(35) Wantanabe, T.; Tanimoto, Y.; Nakagaki, M.; Hiramatsu, M.; Sakata, T.; Nagkura, S. *Bull. Chem. Soc. Jpn.* **1987**, *60*, 4163−4165.
(36) Hinds, G.; Coey, J. M. D.; Lyons, M. E. G. *J. Appl. Phys.* **1998**, *83*, 6447−6449.
(37) Coey, J. M. D.; Hinds, G.; Lyons, M. E. G. *Europhys. Lett.* **1999**, *47*, 267−272.
(38) Mogi, I.; Okubo, S.; Nakagawa, Y. *J. Phys. Soc. Jpn.* **1991**, *60*, 3200−3202.
(39) Takahashi, F.; Sakai, Y.; Tamura, T. *Electrochem. Acta* **1983**, *28*, 1147−1151.
(40) O'brien, R.; Santhanam, K. S. V. *J. Appl. Electrochem.* **1997**, *27*, 573−578.
(41) Shannon, J. C.; Gu, Z. H.; Fahidy, T. Z. *J. Electrochem. Soc.* **1997**, *144*, L314−L316.
(42) Bird, R. B.; Stewart, W. E.; Lightfoot, E. N. *Transport Phenomena*; J. Wiley & Sons: New York, 1960.
(43) Zoski, C. G. In *Modern Techniques in Electrochemistry*; Vanysek, P., Ed.; John Wiley & Sons: New York, 1996.
(44) *Microelectrodes: Theory and Application*; Montenegro, M. I., Quieros, M. A., Daschbach, J. L., Eds.; Kluwer Acadmeic: Boston, MA, 1991.
(45) Kohno, J.; Mafume, F.; Kondow, T. *J. Phys. Chem. A* **2000**, *104*, 243−248.
(46) Mafume, F.; Kohno, J.; Kondow, T. *J. Phys. Chem.* **1996**, *100*, 10041−10045.
(47) Potje-Kamloth, K.; Janata, J.; Josowicz, M. *Ber. Bunsen-Ges. Phys. Chem.* **1989**, *93*, 1480−1485.

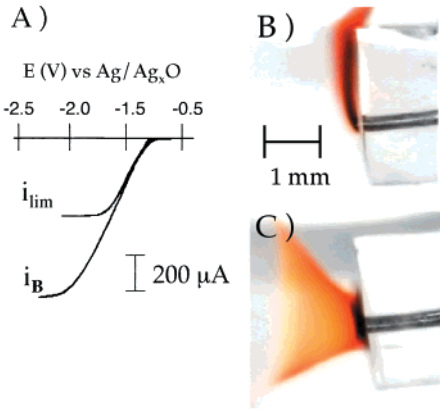

Figure 1. (A) Voltammetric response corresponding to the 1-e$^-$ reduction of NB at a 250-μm-radius Pt disk electrode in a CH_3CN/0.2 M [*n*-Bu_4N]-PF_6 solution containing 0.5 M NB. The steady-state voltammetric limiting currents in the absence (i_{lim}) and presence (i_B) of a 1.0-T magnetic field are indicated on the curve. The corresponding flow patterns are shown in the video-enhanced images: (B) natural convection in absence of the magnetic field and (C) magnetic field-induced vortex flow. The orange-red color corresponds to the radical anion, $NB^{\bullet-}$, generated at the electrode surface.

vernier micrometers (Newport). Video images of flow patterns were recorded by a Panasonic WCP230 color video camera and converted to digital files by use of Ulead Systems MediaStudio Pro software.

Results and Discussion

We report observations of MHD flow tubes, pulsed flow, and circular sheet flow that occur within the gap defined by two Pt microdisk electrodes oriented in a face-to-face configuration. These new forms of MHD flow are driven by magnetic forces that are generated by the passage of Faradaic current at the surfaces of the two microdisk electrodes. Section I describes the origin of the magnetic forces and vortex flow at a single microdisk electrode. The description of different types of MHD flow in the dual-electrode configuration is presented in sections II and III.

I. Magnetic Forces and Vortex Flow at a Single Pt Microdisk. The steady-state voltammetric response of a 250-μm-radius Pt microdisk in a CH_3CN solution containing 0.5 M nitrobenzene (NB) and supporting electrolyte (0.2 M [*n*-Bu_4N]-PF_6) is shown in Figure 1A. Sigmoid-shaped voltammograms with limiting currents i_{lim} and i_B, respectively, are obtained in the absence and presence of a 1-T magnetic field, applied orthogonal to the electrode surface. The voltammetric response arises from the 1-e$^-$ reduction of NB, yielding the brightly orange-red radical anion, eq 2. In a dilute solution of the redox-

$$NB + e^- \rightleftharpoons NB^{\bullet-} \qquad (2)$$

active species and in the absence of a magnetic field, the steady-state limiting current at an inlaid microdisk electrode is given by eq 3, where n is the number of electrons transferred per

$$i_{lim} = 4nFDC^*a \qquad (3)$$

molecule, F is Faraday's constant (C/mol), D (cm^2/s) and C^* (mol/cm^3) are the diffusion coefficient and concentration of the redox species, respectively, and a is the electrode radius.[48] Equation 3 describes the rate at which NB is transported by diffusion from the bulk solution to the electrode surface. As previously shown,[49] the transport-limited current measured at inlaid microdisk electrodes also contains a significant contribution from natural convection whenever the redox species is present in relatively high concentrations, as is the case here for experiments in 0.5 M NB solution. Video-enhanced images of the transport of the orange-red NB anion in the solution adjacent to the Pt microdisk allow flow patterns due to natural convection (at $\mathbf{B} = 0$, Figure 1B) and the magnetic-induced flow (at $\mathbf{B} = 1$ T, Figure 1C) to be easily observed. As demonstrated by Figure 1B, natural convection by itself results in a steady upward flow of solution across the microelectrode surface. The natural convection is due to the density of the depletion layer created by the Faradaic reaction being slightly less than that of the bulk solution, resulting in the solution rising under the influence of gravity. The upward flow increases the rate of transport of NB from the bulk solution to the electrode surface, resulting in a mass-transfer-limited current greater than that predicted by eq 3.

When the 1-T magnetic field is applied orthogonal to the electrode surface, Figure 1C, the electrogenerated $NB^{\bullet-}$ is transported away from the electrode in a spiral path along the surface of a vortex. This unusual transport phenomenon arises from *rotational flow localized along the circumference* of the inlaid disk. To understand the origin of this flow, consider the time-independent Navier−Stokes equation, eq 4, describing velocity of a fluid element as a function of external forces. In

$$\rho(v\cdot\nabla)v = \eta\nabla^2 v + \rho g + \nabla P + \mathbf{J}\times\mathbf{B} \qquad (4)$$

eq 4, ρ and η are the local density and viscosity of the fluid, v is the velocity, P is the pressure, and g is the gravitational acceleration constant.[49,50−52] In the experiments reported here, ∇P can be ignored since there are no pressure gradients in the vicinity of the electrode. When the magnetic force is much smaller than the gravitational force (i.e, $\rho g \gg \mathbf{J}\times\mathbf{B}$), convective mass transport will be dominated by natural convection and the viscous restoring force, $\eta\nabla^2 v$. The fluid motion will be parallel or antiparallel to g, depending on the density of the solution in the depletion layer relative to that of the bulk solution. On the other hand, if $\rho g \ll \mathbf{J}\times\mathbf{B}$, then eq 4 predicts that the magnetic force will induce a rotational flow in which the local direction of flow is orthogonal to both **J** and **B**.

Figure 2 schematically depicts the interaction of **B** and **J** at the inlaid disk electrode. Linear transport of $NB^{\bullet-}$ occurs across the central region of the electrode, while a radial flux is maintained at the disk edges, Figure 2A. In this situation, $\mathbf{F}_{MHD}$ vanishes over much of the central region of the electrode, since **B** and **J** are parallel, Figure 2B. Near the edge of the electrode, the radial outward flux of $NB^{\bullet-}$ through the uniform field requires that $\mathbf{F}_{MHD}$ remain finite. Using the right-hand rule to evaluate the vector cross product of **J** and **B**, it is readily demonstrated that $\mathbf{F}_{MHD}$ is tangential to the electrode circumference, resulting in localized rotational flow along the edge of the electrode, Figure 2C.

Although not apparent in the image of Figure 1C, real-time video imaging of the depletion layer regions clearly reveals that

(48) Saito, Y. *Rev. Polag. Jpn.* **1968**, *15*, 177−187.
(49) Gao, X.; Lee, J.; White, H. S. *Anal. Chem.* **1995**, *67*, 1541−45.
(50) Truesdell, C. *The Kinematics of Vorticity*; Indiana University Press: Bloomington, 1954.
(51) Ockendon, H.; Ockendon, J. R. *Viscous Flow*; Cambridge Press: New York, 1995.
(52) Kleinstreuer, C. *Engineering Fluid Dynamics: An Interdisciplinary Systems Approach*; Cambridge University Press: New York, 1997.

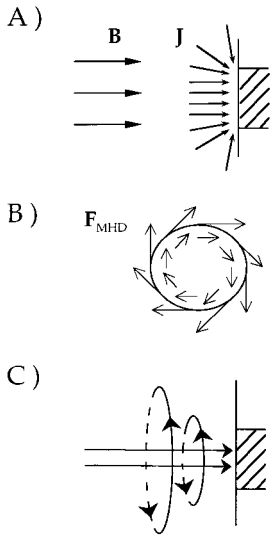

Figure 2. Schematic drawing depicting (A) the magnetic field (**B**) and the flux (**J**) of positive current (side view), (B) the resulting magnetic force ($\mathbf{F}_{MHD} = \mathbf{J} \times \mathbf{B}$) (top view), and (C) the resulting flow of solution. At steady state, the inward flow of solution from the bulk to the electrode surface balances the outward-directed vortex flow.

solution flow occurs from the bulk solution to the electrode along streamlines centered through the middle of the vortex, as depicted in Figure 2C. The inward flow through the center of the vortex balances the outward flow originating at the electrode circumference, bringing fresh solution to the electrode surface. This inward-directed flux through the center of the vortex is responsible for the enhanced current at the microdisk in the presence of the magnetic field.

To obtain a semiquantitative description of the vortex flow, we have used a small Pt microprobe electrode (radius = 25 μm) to map the convective flux of NB and $NB^{\bullet-}$. In these experiments, a steady-state vortex flow is first established at the larger Pt microdisk electrode, and the microprobe electrode is then slowly scanned through the flow field while held at a potential to either oxidize $NB^{\bullet-}$ ($E = -0.5$ V) or reduce NB ($E = -1.5$ V) at the mass-transfer-limited rate. The experiment is similar to a classic rotating ring−disk electrode experiment, in which the outer ring is used to collect products generated at the inner disk.

Figure 3A shows plots of the microprobe current, i_t, as the microprobe is scanned through the vortex in a direction parallel to the Pt microdisk surface (the dashed arrow in Figure 3A shows the path of the microprobe). Figure 3B shows a plot of i_t vs position, z, as the microprobe is scanned at a distance of ~0.3 mm away from the microdisk surface, while biased at $E = -0.5$ V in order to oxidize $NB^{\bullet-}$ that is generated at the Pt microdisk. The plot of i_t vs z displays sharp peaks in the i_t vs z plot at $z = 150$ and 700 μm, each corresponding to a distance of ~250 μm away from the center of the microdisk (located approximately at $z = 400$ μm). The appearance of the peaks indicates that $NB^{\bullet-}$ is confined to the edges of the vortex. More precisely, the increase in i_t results from the convective transport of $NB^{\bullet-}$, which is expressed as Cv, where C and v are, respectively, the local concentration of $NB^{\bullet-}$ and the local fluid velocity. The width of the peaks in the i_t vs z plot indicates that the thickness of the vortex wall, defined by regions where Cv is finite, is less than 50 μm. Smaller peaks in the plot of i_t vs z (Figure 3b) are present at ca. 75 μm from the center of each

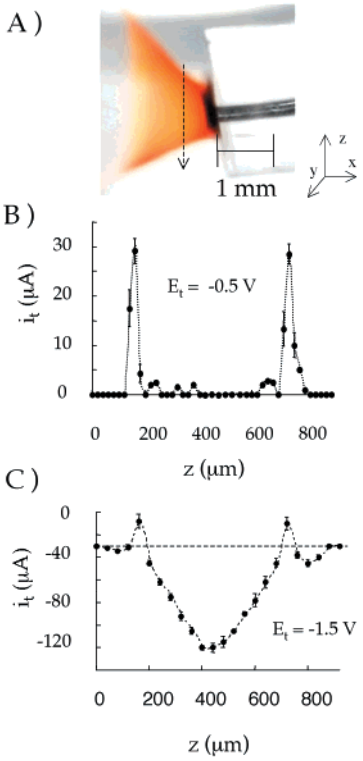

Figure 3. (A) Video micrograph of the vortex flow pattern at a 250-μm-radius Pt disk electrode that is oriented orthogonal to a 1.0-T field. (B) Current (i_t) vs position (z) corresponding to the detection of $NB^{\bullet-}$ at the Pt microprobe electrode, biased at −0.5 V vs Ag/Ag_xO, to *oxidize* electrogenerated $NB^{\bullet-}$. The dashed arrow in (A) shows the path of the microprobe electrode during collection of data presented in (B). Peaks in i_t at $z = 180$ and 720 μm correspond to the vortex edge where the concentration of $NB^{\bullet-}$ is high. (C) Current (i_t) vs position (z) for the *reduction* of NB at the microprobe electrode, biased at a potential of −1.5 V. Increase in cathodic current at $z = 400$ μm is due to inward MHD flow of bulk solution, which increases the rate of molecular transport of NB to the Pt microprobe electrode. The dashed line in (C) corresponds to baseline current ($i_t = \sim 33$ μA) at the microprobe electrode in the bulk solution, far from the surface of the Pt disk.

of the larger peaks, suggesting that the structure of the vortex wall is more complex than a single layer of rotating fluid.

Figure 3C presents the map of the convective flux of the reactant, NB, along the same path in Figure 3A. Here, the baseline current, measured far from the microdisk surface, has a nonzero value (~ −40 μA), since the species being detected (NB) is present in the bulk solution. There are several interesting features in the plot of i_t vs z, Figure 3C. First, sharp decreases in i_t at $z = 150$ and 700 μm, corresponding to a decrease in the convective flux of NB, are observed *within the walls* of the vortex. Since the fluid velocity is higher in this region than in the bulk, the result demonstrates that the concentration of NB in the vortex walls is significantly lower than in the bulk; i.e., the vortex walls are depleted of the electrochemical reactant. This is not altogether unexpected since the fluid in this region originates at the electrode surface where NB is reduced. Second, i_t is approximately three times larger at the center of the vortex than in the bulk solution. Since the concentration of NB in the region cannot be larger than that in the bulk, the result suggests that the increase in current is due to convective flow. The nature of this convective flow is described in the following section.

II. MHD Flow Tubes. To obtain a more quantitative description of the flow profile inside the vortex, experiments

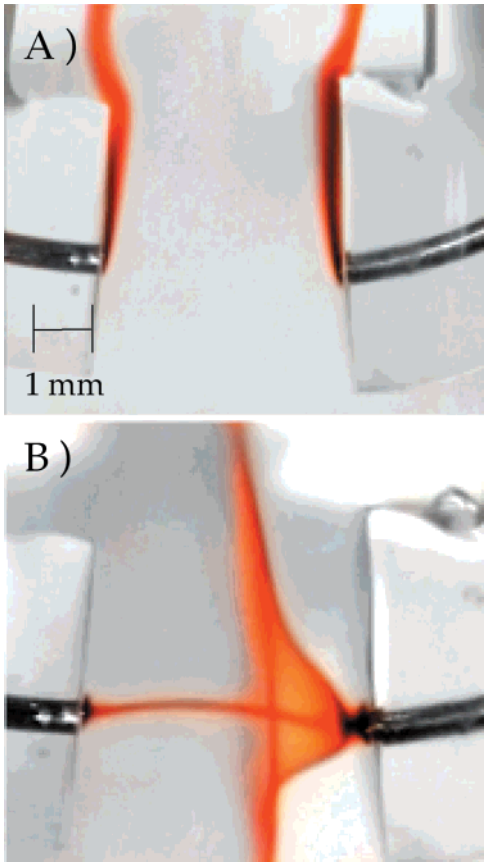

Figure 4. Video micrographs of flow patterns between two 250-μm-radius Pt disk electrodes in a dual-electrode configuration. (A) Gravity-driven flow in the absence of a magnetic field ($\mathbf{B} = 0$). (B) MHD flow at $\mathbf{B} = 1.0$ T. In (B), $NB^{\bullet-}$ that is electrogenerated at the left-side electrode flows across the gap in a flow tube, driven by the vortex flow of the ride-side electrode. Measurements were performed in a CH_3CN/0.2 M [n-Bu_4N]PF_6 solution containing 1.0 M NB, with both electrodes biased at -2.5 V vs Ag/Ag_xO.

were performed in which a second Pt microdisk electrode (radius $= 250$ μm) was positioned several millimeters in front of the first microdisk, such that the electrode surfaces are facing one another. The purpose of the second Pt microdisk is to act as a source of the highly colored $NB^{\bullet-}$, which serves as a marker to image the flow pattern inside the vortex of the opposing electrode. Figure 4A shows the face-to-face dual-electrode geometry and the distribution of $NB^{\bullet-}$ in the absence of the magnetic field. As with a single electrode, natural convection results in an upward flow of the depletion layer solution. When a magnetic field of 1 T is applied orthogonal to the electrode surfaces, Figure 4B, a flow tube is observed that spans the gap between the two electrodes. In this specific example, the flow originates at the left-side electrode and passes through the center of the vortex to the right-side electrode. The direction of the flow, and the electrode at which vortex flow occurs, can be reversed. For instance, if the right-hand electrode is disconnected, the flow tube will disappear, and a vortex flow pattern will spontaneously occur at the left-side electrode. Reconnecting the ride-side electrode will result in a flow tube, with the direction of flow the opposite of that shown in Figure 3B. The flow tubes have diameters ranging from 25 to 100 μm and can span the gap of electrodes separated by distances as large as 2 cm. By imaging the motion of particles trapped in the flow tube, we have estimated the fluid velocity to be $\sim$2.5 cm/s. The flow tubes are not unique to the NB system. Similar flow tubes in

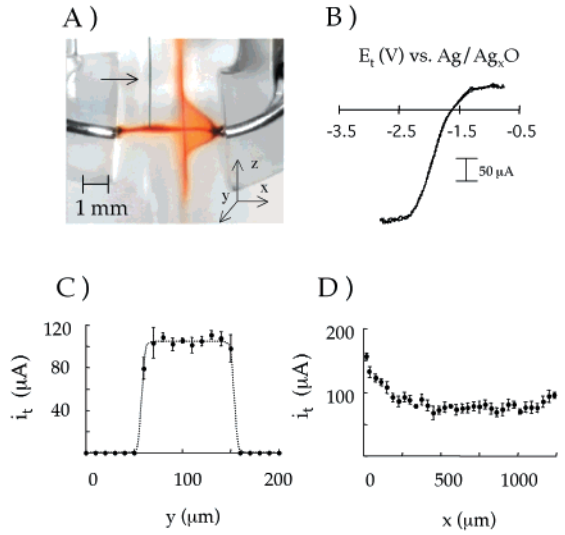

Figure 5. (A) Video micrograph of the Pt microprobe electrode (indicated by the arrow) positioned in the focused beam (experimental conditions the same as in Figure 4). (B) Steady-state voltammogram at the Pt microprobe within the flow tube (cathodic and anodic currents corresponding, respectively, to the reduction of NB and oxidation of $NB^{\bullet-}$). (C) Current (i_t) vs position (y) as the Pt microprobe electrode is scanned across the waist of the flow tube while held at a potential of -0.5 V in order to detect $NB^{\bullet-}$. (D) Current (i_t) vs position (x) along the length of the flow tube, where $x = 0$ corresponds to the surface of the left-side electrode.

the dual-electrode geometry have also been observed in aqueous solutions during the oxidization of Br^-. In these experiments, electrogenerated Br_2 is transported between the electrodes within the flow tube. In principle, the phenomena reported here can be obtained with any redox system, since $\mathbf{F}_{MHD}$ (eq 1) does not depend on the chemical nature of the redox species.[53]

The convective flux inside the flow tube was characterized in a series of experiments using the small Pt microprobe to map the distributions of NB and $NB^{\bullet-}$. Figure 5A shows an image of the Pt microprobe positioned inside a flow tube between the two Pt microdisks separated by $\sim$0.35 cm. The voltammetric response of the microprobe electrode, Figure 5B, shows both cathodic and anodic currents, corresponding to the reduction and oxidation, respectively, of NB and $NB^{\bullet-}$. The latter species is generated at the left-side microdisk electrode and transported to the microprobe electrode, where it is detected.

The width of the flow tube can be precisely measured by scanning the microprobe electrode through the tube. Figure 5C shows a plot of i_t vs y for the oxidation of $NB^{\bullet-}$, obtained by scanning the microprobe through the waist of the flow tube (see x, y, z coordinate system defined in Figure 5A). The microprobe current increases sharply from a negligibly small background value to $\sim$100 μA as the microprobe enters the tube, indicating a very sharp boundary ($<$10 μm) between the stagnant solution and the solution flowing inside the tube. From the plot of i_t vs y, the width of the flow tube shown in Figure 5 is measured to be ca. 95 μm. The ability to transport chemical species inside the flow tube without losses to diffusion or turbulent mixing with the surrounding fluid was quantified by scanning the microprobe in the x-direction along the length of the tube, Figure 5D. Although there is a drop in anodic current as the electrode initially moves away from the left-side electrode surface (at x

(53) In eq 1, the force is proportional to the current flux (**J**) that is carried primarily by supporting electrolyte ions. Thus, a magnetic force is generated even if both the redox reactant and product are uncharged.

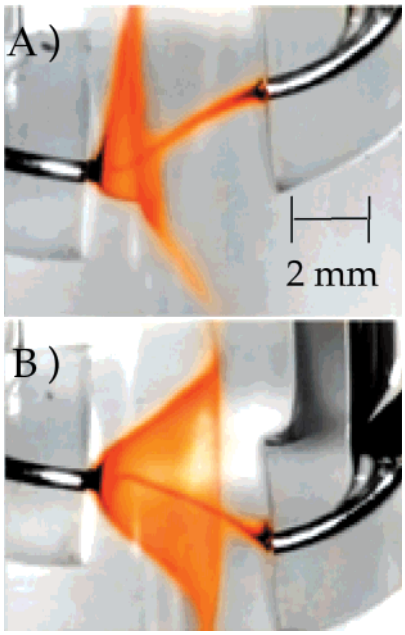

Figure 6. Video micrographs of a flow tube oriented (A) downward and (B) upward by varying the positions of the electrodes. Other conditions are the same as in Figure 4.

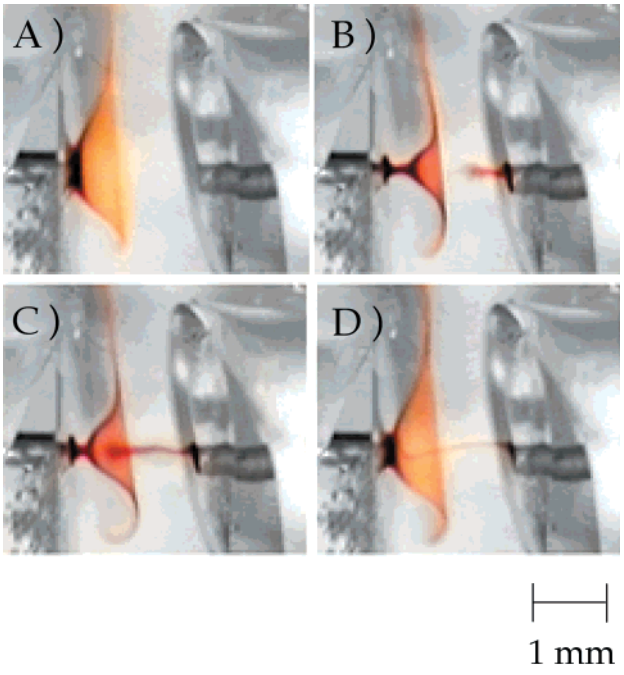

Figure 7. Video micrographs showing the transient transport of ca. 10^{-11} mol of $NB^{\bullet-}$ across the electrode gap at (A) 0.0, (B) 0.25, (C) 0.5, and (D) 0.75 s following a 5-ms pulse between −0.5 and −2.5 V at the left-side electrode. Other conditions are the same as in Figure 4.

$= 0$), the magnitude of i_t at larger distances remains relatively constant. This finding suggests that the flow tube system can be used to *quantitatively* transfer molecules over macroscopic lengths through a condensed phase.

The molecular beam can be focused in a variety of directions, depending on the relative position of the facing Pt electrodes. Figure 6, parts A and B, shows the downward and upward transport of $NB^{\bullet-}$, respectively, between two Pt electrodes. The direction of the flow tube in these experiments is determined solely by the relative positions of the two Pt microdisk electrodes.

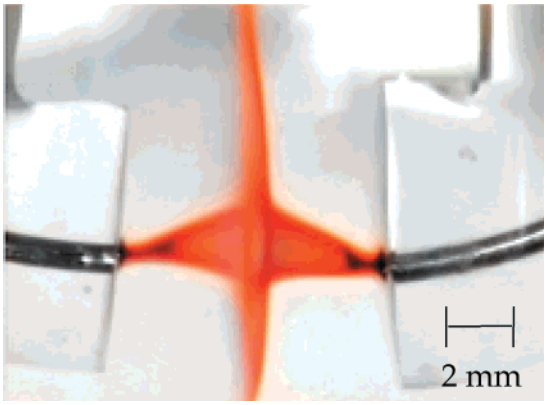

Figure 8. Video micrograph of a steady-state rotating circular sheet of solution (20 μm thick and 1 cm wide, rotating at $f = 0.08\ s^{-1}$) between the two Pt microdisk electrodes. Electrode potentials were set to a value on the limiting current plateau. Other conditions are the same as in Figure 4.

III. Pulsed Transport and Rotating Sheets of Fluid. "Packets" of $NB^{\bullet-}$ may also be transported through the solution in pulsed flow. Figure 7 shows a time sequence of images (0.25 s elapsed time between each image) in which a small quantity of $NB^{\bullet-}$ is transported from the right-side electrode through the vortex to the left-side electrode. Here, $NB^{\bullet-}$ was electrogenerated by stepping the potential of the right electrode from 0.0 to −2.5 V for 5 ms, generating $\sim 2 \times 10^{-11}$ mol of $NB^{\bullet-}$. The sequence of images shows that the molecules reach the opposing electrode surface in ∼0.75 s, corresponding to an average fluid velocity of 2 mm/s.

Other interesting flow patterns can be established by controlling the electrode potential. For instance, when the potential of each microelectrode is simultaneously applied, the flow vortices from each electrode intersect at the middle of the gap, creating a thin rotating sheet of solution. Figure 8 shows a ∼20-μm-thick, ∼2-cm-diameter sheet of fluid created between the surfaces of two 250-μm-radius electrodes. From video images, the frequency of the sheet rotation is estimated to be $0.08\ s^{-1}$ at a field strength of 1 T. The rotational frequency can be controlled by adjusting the external field, with larger fields producing higher rotational rates. Magnetic fields as low as 0.25 T have been used to maintain sheet flow for periods of up to 4 h.

Conclusion

The results reported here demonstrate the controlled transport of molecules through a liquid phase in microscopic flow patterns that are defined using an external magnetic field. While the examples of tube flow and pulsed flow have no immediate practical application, there is presently considerable interest in microfluidic systems for controlled delivery of small quantities of chemicals. Our work establishes that fundamental principles learned from electrochemistry and the study of macroscopic MHD flows can be applied in a much smaller spatial regime to generate new types of flow capable of transporting molecular species across macroscopic distances in a free solution (no surfaces).

Acknowledgment. This work was supported by the Office of Naval Research.

JA016544Y